

## Providing Advanced Scientific Knowledge by Concentrating Expertise

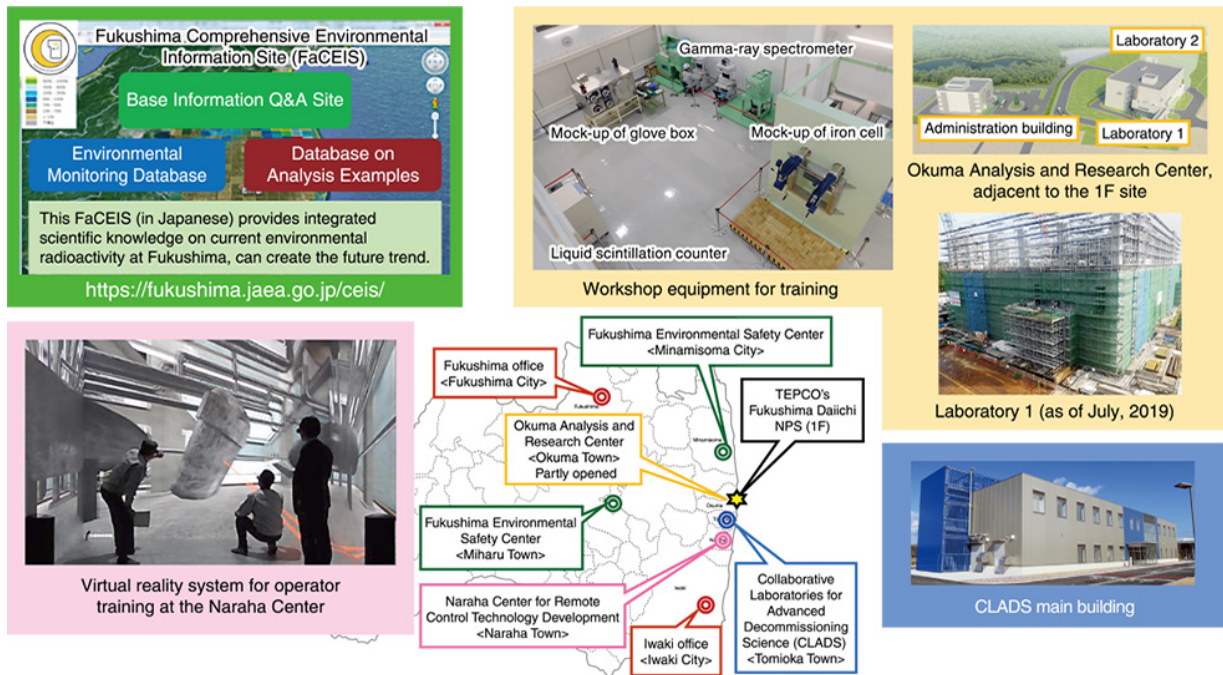


Fig.1-1 Sector of Fukushima research and development: fields and activities

As a comprehensive R&D institute in the field of nuclear energy, JAEA has been supporting the post-accident environmental restoration and decommissioning of the TEPCO's Fukushima Daiichi NPS (1F) (Fig.1-1).

The Collaborative Laboratories for Advanced Decommissioning Science (CLADS) is a research hub for R&D on decommissioning. JAEA has been studying to clarify the debris distribution inside reactors toward a retrieval of nuclear fuel debris (Topic 1-1). In order to understand the debris characteristics, JAEA has evaluated their mechanical characteristics by computer simulation (Topic 1-2) and investigated experimentally the behavior of boron that causes the debris to harden (Topic 1-3).

To ensure radiation protection during debris retrieval, JAEA has been developing the nuclear criticality evaluation method for debris (Topic 1-4) as well as an alpha-ray monitor that is available inside 1F buildings where temperature and humidity have not been controlled yet (Topic 1-5). JAEA also is studying the storage, treatment, disposal and reuse of liquid or solid types of radioactive wastes generated from decommissioning work (Topics 1-6–1-9). Additionally, a dedicated lab in collaboration with universities and industries was established in FY2019 to develop human resources and concentrate expertise toward future 1F decommissioning (Fig.1-1, bottom right).

The Naraha Center for Remote Control Technology Development was also established as a facility for the development and demonstration of remote control devices contributing to 1F decommissioning work. Here, virtual reality systems prepared for operator training (Fig.1-1, bottom left) and robot simulators for decommissioning work (Topic 1-10) are under development. The facilities are available for external researchers. For example, the International Research Institute for Nuclear Decommissioning (IRID) has performed a development of technology for Water Circulation Systems in Primary Containment Vessel (Full-scale Test) using this center.

The Okuma Analysis and Research Center is designed to analyze and characterize radioactive wastes and nuclear fuel debris for the development of long-term waste management. Laboratory 1, which will deal with low-to-medium-level radioactive waste

including rubble and secondary waste, is under construction. Laboratory 2, in the design phase, will deal with high-level radioactive material such as fuel debris. To ensure analysis work in the future, JAEA is training for analyzing work at workshop in Administration Building and so on (Fig.1-1, top right).

These centers will contribute to the decommissioning of 1F and are regarded as decommissioning-related facilities that will play a part in the Fukushima Innovation Coast Framework.

The Fukushima Environmental Safety Center has performed R&D for the environmental restoration. For the long-term assessment of transport of radioactive cesium in the environment, its discharge of radioactive cesium in the dissolved form from the overland to rivers was investigated through long-term concentration monitoring in river water (Topic 1-11) and computer simulations (Topic 1-12). The center has developed a technique to evaluate the vertical distribution of radioactive cesium in pond subsoil based on the gamma-ray spectra (Topic 1-13). JAEA discovered a phenomenon in which radionuclides drastically sink to the deep ocean due to the serpentine current (Topic 1-14). JAEA has promoted the technological development of environmental radiation monitoring and mapping to establish rapid evaluation methods for the distribution of radionuclides. JAEA has succeeded in the definition of radiation exposure dose evaluation for residence at the zone designated for reconstruction and recovery by developing the inverse analysis method for airborne radiation monitoring (Topic 1-15). JAEA has also showed the effective dose estimation at the zone designated for reconstruction and recovery using new approaches for the evaluation of the effective dose (Topic 1-16), and developed an evaluation system to create detailed 3D models of residential areas to improve the precision of calculations of air dose rate distributions (Topic 1-17).

The R&D results are published on an information website (Fig.1-1, top left), contributing to building residents' sense of security and studying the measures for municipalities.

Furthermore, JAEA is contributing to Fukushima's revitalization through R&D activities with development of human resources by building networks with regional industries, research institutes, and educational institutes.

# 1-1 Estimate the State of the RPV and PCV after a Severe Accident

## — Upgrading of the Comprehensive Identification of Conditions Inside Reactor —

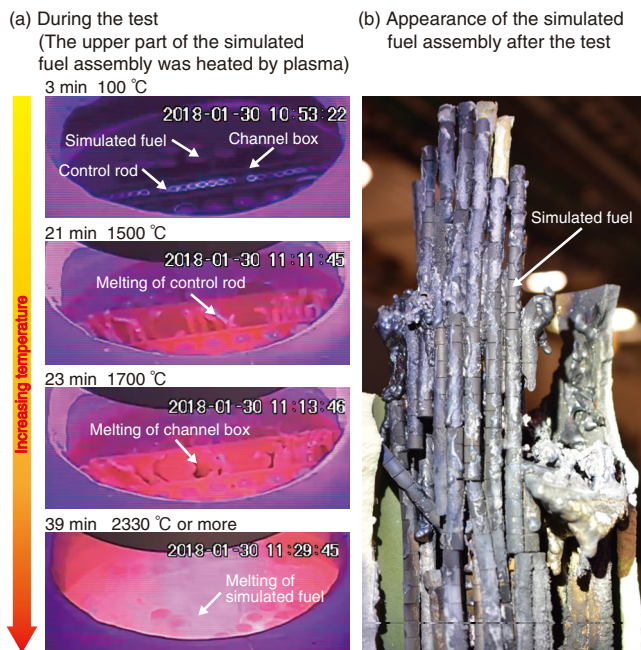


**Fig.1-2 Core-material melting and relocation (CMMR) test**  
The simulated fuel assembly at the top was heated by plasma. A  $ZrO_2$  pellet was used, rather than  $UO_2$ . (a) A downward flow was observed in order of materials with lower melting points. (b) The simulated fuel retained the column shape until its melting temperature.

The decommissioning of the TEPCO's Fukushima Daiichi NPS (1F) has been underway since its severe accident (SA) in March 2011. Estimating and comprehending the state of the remaining fuel debris and fission products inside the nuclear reactor is essential for this process. However, understanding the state the reactor pressure vessel (RPV) and primary containment vessel (PCV) is extremely difficult after an accident, as direct observation of the reactor interior is difficult due to the high radiation environment. Additionally, as Unit 1–Unit 3 at 1F lost their cooling functions during the tsunami, as well as their direct-current electric power supply, measurements cannot easily be collected from the onboard meters. Thus, information measured during the accident progression is in short supply. To make up for this lack of accident information, SA models based on knowledge of the Three Mile Island (TMI-2) accident and some experimental work can be applied. However, core degradation in a boiling water reactor (BWR) like the 1F has not been comprehensively studied. Since the TMI-2 accident, many researchers have focused on the initial core melting process and aspects related to the rupture of the pressure vessel in a pressurized water reactor (PWR). The differing structure between a BWR and a PWR may result in different core damage, melting, and slumping in the 1F accident.

In the “Upgrading of the comprehensive identification of conditions inside reactor” project, core-material melting and relocation (CMMR) tests were conducted to understand the collapsing, melting and relocation of core materials during 1F accident (Fig.1-2). A fuel assembly simulating the core of a BWR

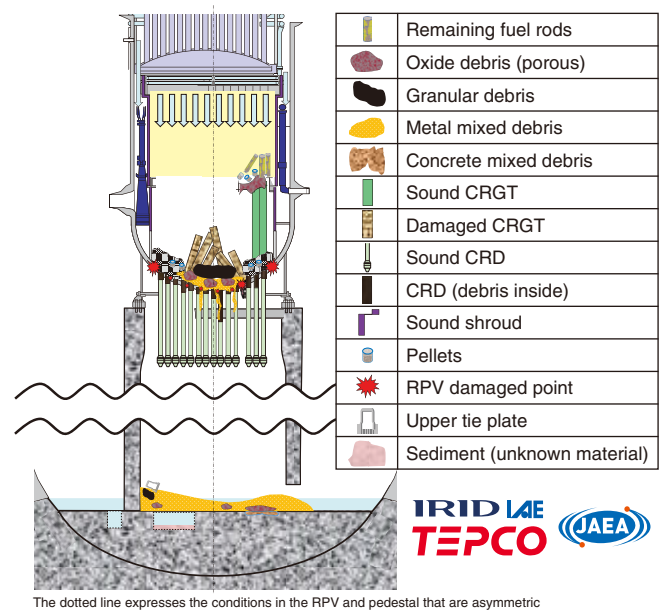


**Fig.1-3 Estimated debris distribution and the RPV and PCV conditions in Unit 2**

The state of residual fuel in the lower plenum were estimated via the results presented in Fig.1-2.

using  $ZrO_2$  pellets rather than fuel pellets was heated by high-temperature plasma. The simulated fuel assembly at the top was heated above the oxide melting temperature, not yet achieved in prior tests simulating the BWR system, reproducing the axial temperature gradient at the initial stage of core material melting and relocation in the 1F accident. The results indicated that the macroscopic gas permeability of the heated core remained intact until the ceramic fuel melting point. Furthermore, as hot fuel remained in columns, effective fuel relocation, i.e., the removal of hottest fuel from the middle of the core to heat the support structure, was shown to be unlikely. These results will assist in the development of better BWR-specific SA progression models. The 1F plant data collected from CMMR testing, SA analysis, and the 1F internal investigation was then further analyzed to estimate post-accident reactor conditions. The resulting estimation of debris distribution in the Unit 2 RPV/PCV is shown in Fig.1-3.

Future work will involve analyzing the data from 1F internal investigations to further understand reactor conditions and upgrade estimated diagrams of debris distribution in the RPV and PCV. These estimations will contribute to the development of effective policies for removing fuel debris from the 1F site.

This work was the result of the subsidy for Project of Decommissioning and contaminated Water Management, “Upgrading for Identifying Comprehensive Conditions inside the Reactor”, supported by the Agency of Natural Resources and Energy (ANRE), the Ministry of Economy, Trade and Industry (METI), Japan.

### Reference

Yamashita, T. et al., The CMMR Program: BWR Core Degradation in the CMMR-4 Test, Proceedings of the 9th European Review Meeting on Severe Accident Research (ERMSAR 2019), Prague, Czech Republic, 2019, 012, 13p.

## 1-2 Numerical Evaluation of Fuel Debris Hardness

### — First-Principle Calculation of the Mechanical Properties of Fuel Debris —

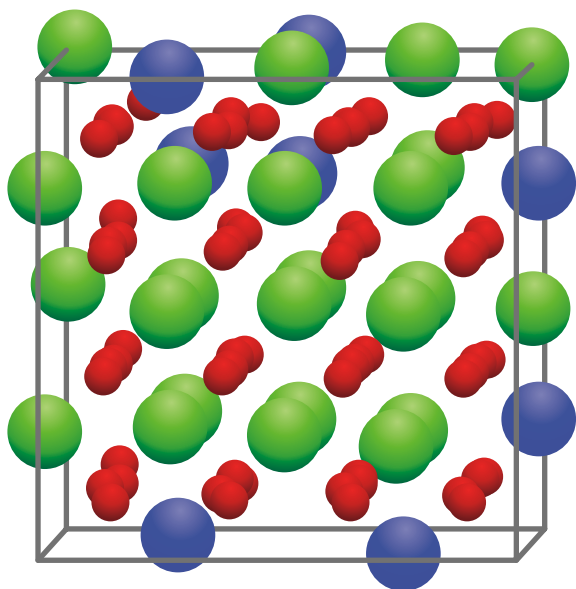


**Fig.1-4 Crystalline structure of uranium-zirconium oxide**  
This structure, constructed by 24 uranium atoms (●), 8 zirconium atoms (●), and 64 oxygen atoms (●), represents one of the crystalline structures used in the calculations.

Proper removal of fuel debris formed from melting fuel is necessary to the safe decommissioning of the TEPCO's Fukushima Daiichi NPS (1F). To remove debris safely, its mechanical properties should be understood, including the hardness, elastic modulus, and fracture toughness. As these have not yet been studied in detail, property estimation using simulated debris is essential. Furthermore, since the detailed components of the debris are not yet completely understood, a vast array of simulated debris must be created and analyzed, thus requiring extensive time and costs. Estimating the mechanical properties of debris with numerical models could therefore greatly reduce costs and help debris removal efforts.

As such, an atomic nuclear model was developed to simulate the mechanical properties of uranium-zirconium oxide (Fig.1-4), the main component of the fuel debris. A first-principles calculation method was adopted, as this reliable method does not require any empirical parameters. The calculated Young's

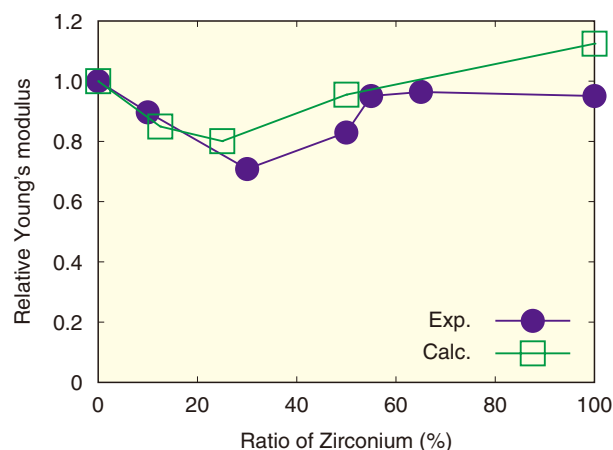


**Fig.1-5 Relative Young's modulus of uranium-zirconium oxide**  
Here, the horizontal axis corresponds to the ratio of zirconium atoms to the sum of uranium and zirconium atoms, and the vertical axis shows the relative Young's modulus of uranium-zirconium dioxide to that of uranium dioxide. The closed circles and open squares represent experimental and calculated results, respectively.

modulus, one of elastic moduli, for uranium-zirconium oxides, is shown in Fig.1-5. Prior experimental work has indicated that Young's modulus decreases as the zirconium ratio increases until 25% and increases above 25%. The calculated Young's modulus showed a similar behavior. Analyzing the simulation results, we found that the distortion of the oxygen atom configuration became the greatest at 25%, and reduced the Young's modulus. Thus, this demonstrated another benefit of numerical models: not only can the physical properties be evaluated, but their causes can be elucidated.

This work focused on evaluating the mechanical properties of fuel debris by atomic numerical simulations. However, more information regarding the properties of fuel debris properties is still required. The developed numerical method can support future experimental analysis of fuel debris properties, this contributing to decommissioning activities at 1F.

#### Reference

Itakura, M., Nakamura, H. et al., First-Principles Calculation of Mechanical Properties of Simulated Debris  $Zr_xU_{1-x}O_2$ , Journal of Nuclear Science and Technology, vol.56, issues 9-10, 2019, p.915-921.

# 1-3 Degradation Mechanism of a BWR Control Blade

## — Understanding the Behavior of Boron Compounds during a Severe Accident —

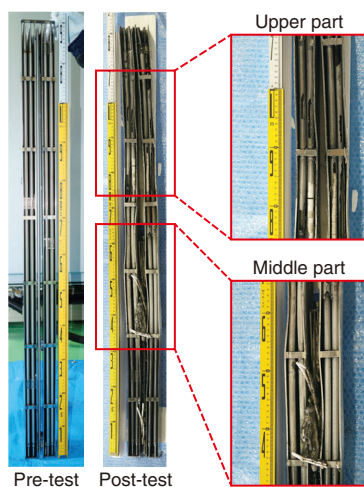


**Fig.1-6 Sample used to simulate a part of a typical Japanese BWR fuel assembly**

After testing, a part of the control blade remained at the top part of the sample. The blockage at the middle was composed of solidified candling sample droplets.

Since the accident at the TEPCO's Fukushima Daiichi NPS (1F), the researchers have aimed to uncover new features of the influence of boron carbide ( $B_4C$ ) on the 1F accident progression. Although boron is necessary in BWR reactors, the presence of  $B_4C$  has led to low-temperature eutectics with Fe, formation of very hard phases with Zr and Cr, and the evaporation in hot steam as B-aerosols.

To support 1F decommissioning by understanding the final redistribution of B and C, a mock-up assembly in the Large-scale Equipment for Investigation of Severe Accidents in Nuclear reactors (LEISAN) facility was designed to recreate the accident conditions of Unit 2 at 1F. The results indicated that the control blade did not melt completely and contained intact  $B_4C$ -granules even at 1500 °C, as shown in Fig.1-6.

Nevertheless, a significant portion of the stainless steel (SS) liquefied (with help of  $B_4C$ ) relocated to lower elevations, and solidified. As a result, the gap between the control blade and channel box was blocked at the test sample elevations where the temperature was roughly 1174 °C–1250 °C.

A schematic representation of the control blade degradation mechanism at an early phase of nuclear accident up to 1500 °C under steam-starved conditions is represented in the Fig.1-7. An analysis of the survived residuals indicated that contact between  $B_4C$  and SS resulted in the formation of Cr-rich carboborides,

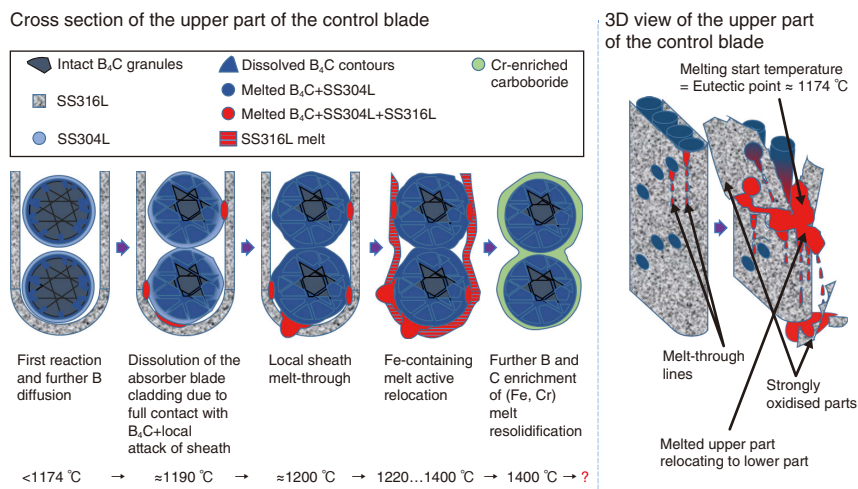


**Fig.1-7 Schematic of the control blade degradation mechanism at an early phase of the nuclear accident under steam-starved conditions**

During an accident conditions B and C can diffuse into the wall of the control rod tube and locally change its internal structure, causes the formation of melt. As the melt becomes further enriched with B and C, it can become Fe-enriched carboboride between the granules of  $B_4C$ , and Cr-enriched carboboride layer surrounding the granules.

which surrounded the  $B_4C$  granules and significantly decreased further B transport outside of the control rod and, thus suppressing the formation of B-aerosols.

The upper residuals were found to be oversaturated with B and C and thus very hard, but fragile. The blockage, containing mostly melts with lower concentrations of dissolved B and C, was hard and robust, thus representing an additional difficulty for 1F decommissioning.

Thus, B and C create the first wave of melt during the early stage of an accident. This solid melt creates robust blockages, representing significant difficulties for decommissioning. The part of the control blade that survived the first melt contained trapped  $B_4C$  protected by the Cr-rich layer with carboborides. Due to encapsulation of  $B_4C$  by high-melting point compounds under Unit 2 accident conditions, direct contact with environment was limited, thus formation of B-aerosols was probably shifted to late phase of the accident, where melting of high-temperature materials can be possible.

This work was part of the project “Advanced Multi-Scale Modelling and Experimental Tests on Fuel Degradation in Severe Accident Conditions”, supported by the Agency of Natural Resources and Energy (ANRE), the Ministry of Economy, Trade and Industry (METI), Japan.

### Reference

Pshenichnikov, A. et al., Features of a Control Blade Degradation Observed *In Situ* during Severe Accidents in Boiling Water Reactors, Journal of Nuclear Science and Technology, vol.56, issue 5, 2019, p.440–453.

# 1-4 Uncertainty Estimation in the Criticality of Nuclear Systems Containing Fuel Debris

## — Development of a Criticality Calculation Method for Randomly Distributed Materials —

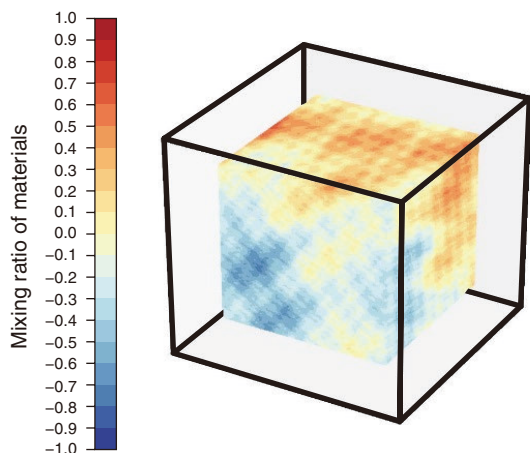


**Fig.1-8 Nuclear system containing hypothetical fuel debris**

An inner cube with a side of 100 cm of fuel debris is surrounded with concrete 20 cm in thickness. Fuel debris is modeled with a mixture of 2 materials such as nuclear fuel and concrete. The brown region shows one material of 100%, and the blue region shows the other material of 100%.

During the accident at the TEPCO's Fukushima Daiichi NPS, fuel debris may have formed from melted nuclear fuels and structural materials such as iron and concrete. Estimating the criticality of nuclear systems containing fuel debris, important to prevent a criticality accident, can be done using computational models for the decommissioning project including defueling. In conventional models, the calculated geometry has been divided into regions small enough to be treated as uniform. However, applying these models to fuel debris systems is difficult, as the isotopic composition varies continuously in space. In addition, conventional analysis required an input of the composition over all regions, which is unknown in fuel debris systems.

As such, a new computational model was developed in which the isotopic composition varies continuously using the Weierstrass function. Users can generate a replica, as shown in Fig.1-8, by inputting the average value and dispersion of the composition and the parameters describing the randomness. Fuel debris is represented as a mixture of two materials, e.g., nuclear fuel and concrete, of which their ratio varies continuously in space. Since a replica is generated stochastically, each replica has a different isotopic composition distribution. Users can calculate the uncertainty due to the unknown distribution of the isotopic composition by calculating criticalities for multiple systems and performing statistical processing.

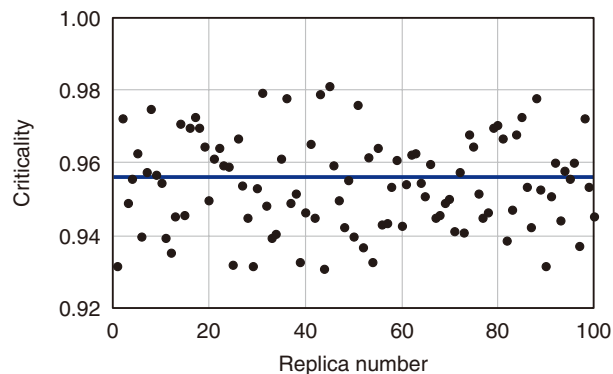


**Fig.1-9 Fluctuation of criticality for a nuclear system containing hypothetical fuel debris**

Fuel debris was assumed to be a mixture of nuclear fuel and concrete (mixing ratio of 1:7) and include an average of 20% stainless steel. Criticality was calculated on the assumption that the content of stainless steel varied randomly and continuously in space between 0% and 40%. The blue line shows the criticality ( $=0.9562$ ) for the nuclear system where the isotopic composition was assumed to be uniform.

The resulting fluctuation of the criticality of a nuclear system containing hypothetical fuel debris is shown in Fig.1-9. A hundred replicas were generated and the criticality was calculated for each replica. The fuel debris was assumed to be a mixture of nuclear fuel and concrete (mixing ratio of 1:7) and included an average of 20% stainless steel. The content rate of stainless steel was assumed to vary randomly and continuously in space between 0% and 40%. In Fig.1-8, the brown region (scale of 1.0) shows the mixture at 0% stainless steel, whereas the blue region (scale of -1.0) shows the mixture with 40% stainless steel. The criticality of a nuclear system with uniform isotopic composition is shown as the blue line in Fig.1-9. One replicated case had a criticality of 0.98. This figure illustrates the importance of not only calculating the criticality for the uniform distribution but also estimating the dispersion due to the non-uniform distribution of stainless steel.

Future work will aim to develop a new model superposed with voxel geometry and the apply the model to a mixture of more than 3 materials to calculate the criticality for the various configuration of complex fuel debris systems. Future work will also involve the development of a Monte Carlo solver to implement and use the developed models easily.

This study was partly sponsored by the Secretariat of the Nuclear Regulation Authority (NRA), Japan.

### References

- Ueki, T., Monte Carlo Criticality Analysis under Material Distribution Uncertainty, *Journal of Nuclear Science and Technology*, vol.54, issue 3, 2017, p.267-279.
- Nagaya, Y. et al., SOLOMON: a Monte Carlo Solver for Criticality Safety Analysis, *Proceedings of 11th International Conference on Nuclear Criticality Safety (ICNC 2019)*, Paris, France, 2019, 9p.

# 1-5 Measuring Alpha-Particle Emitters Flying in Nuclear Facility Buildings

## — A Highly Reliable Alpha Dust Monitor Using a GPS Scintillator Plate —

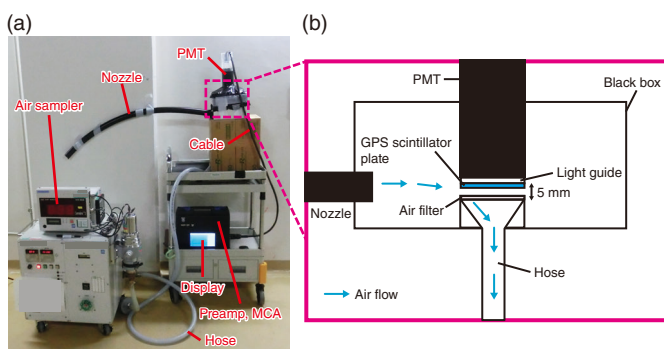


**Fig.1-10 Developed (a) alpha dust monitor (b) and sample holder**  
 The alpha-particle detector was positioned in the sampling holder facing downward, and the detection end was placed in a light-tight box. A nozzle and an air sampler were also connected to the same light-tight box.

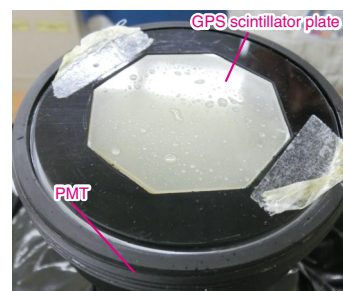


**Fig.1-11 Simulation of the humidity condition**  
 Water was dropped directly onto the GPS plate.

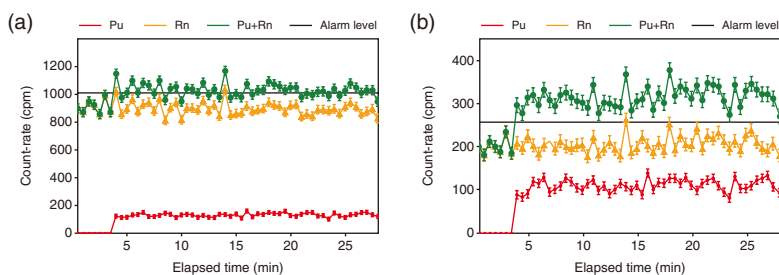


**Fig.1-12 Time variation of counts with 30 s intervals**  
 (a) without and (b) with an energy window

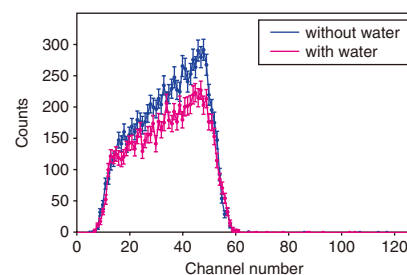


**Fig.1-13 Alpha energy spectra with and without dropping water**

The ratio of the total counts with/without water was 0.84. The peak number of channels without and with water were 47.1 and 47.3 channels, respectively.

A dust monitor with a silicon surface barrier detector (SSBD) was introduced at a nuclear fuel facility to detect the airborne concentration of  $^{238}\text{Pu}$  and  $^{239}\text{Pu}$  released by past accidents. The SSBD energy resolution can distinguish  $^{238}\text{Pu}$  and  $^{239}\text{Pu}$  from naturally occurring radionuclides, such as radon (Rn) progenies (e.g.,  $^{218}\text{Po}$  with a 6.0 MeV alpha particle and  $^{214}\text{Po}$  with a 7.7 MeV alpha particle). However, the SSBD frequently produces false alarms, especially in rooms with high humidity. Under false alarms, workers must evacuate, thus interrupting operations in the room. Thus, a more reliable dust monitor that has a high energy resolution but is more resilient against external noise is required.

Therefore, an alpha-particle spectrometer based on a cerium-doped  $\text{Gd}_2\text{Si}_2\text{O}_7$  (GPS) scintillator plate and a photomultiplier tube (PMT) was developed, as shown in Fig.1-10. The GPS scintillator plate is hexagonal and 50 mm in diameter with a scintillator layer of approximately  $40\ \mu\text{m}$ . The bottom face of the GPS scintillator plate was optically coupled to a PMT (R6233, Hamamatsu Photonics K.K., Hamamatsu, Japan) with a diameter of 3 mm in using an optical grease. The output signal from the PMT is amplified by a preamplifier (5625, Clear pulse CO., LTD., Tokyo, Japan) and transferred to a multi-channel analyzer (MCA; A2731, Clear pulse CO., LTD., Tokyo, Japan). The energy spectrum is then displayed in real-time. The alpha-particle detector was positioned facing downward and the detection end was placed in a black box, which was connected to a nozzle and an air sampler. When the air sampler operates, the

nozzle sucks up the air around the monitor, and any radioactive dust in the air is captured by the filter. The distance between the GPS scintillator plate and the filter was approximately 5 mm to allow for air passage. The  $^{241}\text{Am}$  alpha source, Rn progeny collected on the air filter, and a  $\text{PuO}_2$  particle were measured by our developed dust monitor. Water was dropped directly onto the surface of the GPS plate using a dropper to simulate high-humidity conditions (Fig.1-11).

The resulting energy resolution for 5.5-MeV alpha particles was  $11.9\% \pm 0.2\%$  of the FWHM. A 92% efficiency was achieved, as was a uniform sensitivity. To eliminate Rn progeny counts, an energy window was set with the upper (ULD) and lower (LLD) channels of the Pu sample spectrum. By applying the energy window, the count-rate of the Rn progeny decreased by 77% (Fig.1-12). The resulting alpha spectra with and without dropping water are shown in Fig.1-13 for a measurement time of 5 min. The GPS scintillator plate could be used to measure the alpha spectrum even though the GPS scintillator got wet. The ratio of the total counts with/without water was 0.84. The peak number of channels without and with water were similar: 47.1 and 47.3 channels, respectively.

Overall, the developed dust monitor can be used to conduct alpha-particle spectroscopy despite the presence of water on the surface of the GPS scintillator plate. An alpha dust monitor using a GPS scintillator plate is therefore ideal for detecting alpha-particle emitters in places lacking temperature and humidity controls.

### Reference

Morishita, Y. et al., Development of an Alpha Dust Monitor Using a GPS Scintillator Plate, Radiation Measurements, vol.122, 2019, p.115–120.

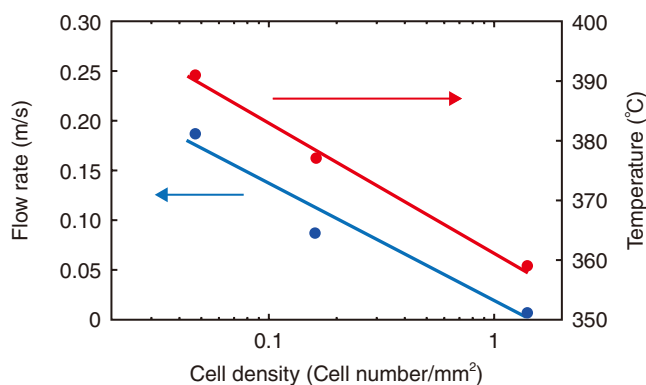
# 1-6 Determination of the Optimum Shape of Hydrogen Recombination Catalysts

## — Hydrogen Elimination Effect Experimentally Verified for Full-Size Equipment —

**Table 1-1 Catalyst specifications**

Several catalysts were prepared to identify the effect of cell density on the catalytic reaction.

Appearance			
Cell density (Cell number/mm <sup>2</sup> )	0.047	0.16	1.4
Cell pitch (mm)	4.6	2.5	0.85
Wall thickness (mm)	0.66	0.43	0.064
Cell length (mm)	3.9	2.1	0.79

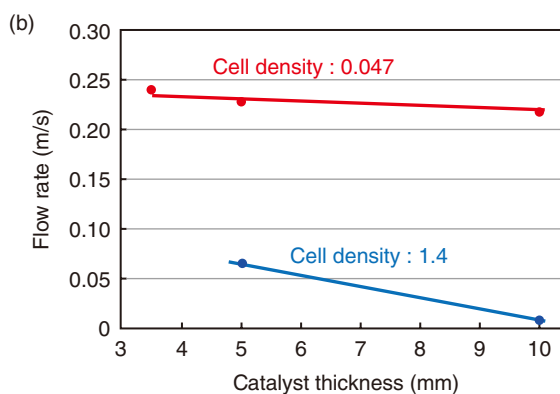
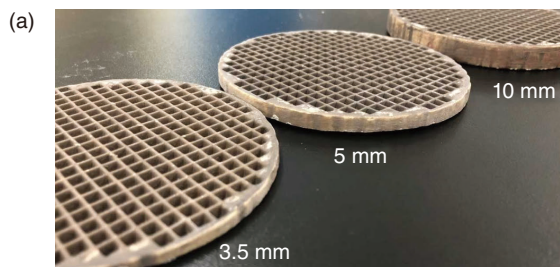

**Fig.1-14 Effect of cell density on the catalytic reaction**

The flow rate and gas temperature were observed when using several catalysts. The flow rate increased as the cell density decreased.

Nuclear fuel waste storage containers generate hydrogen gases due to the radiolysis of water molecules. Hydrogen elimination systems using hydrogen recombination catalysts, which do not rely upon an external electric power, have attracted much attention. The catalysts make a non-explosive reaction between atmospheric oxygen and the generated hydrogen, thus reducing the hydrogen concentration without the use of external electric power.

In this work, hydrogen recombination catalysts were developed based on an automotive catalyst and evaluated for their hydrogen elimination capabilities using full-scale equipment. The equipment used for performing the hydrogen recombination experiments was located at the Forschungszentrum Jülich in Germany and has a sealed cylindrical shape with an inner diameter of 1400 mm and a height of 3700 mm. After the catalyst was loaded, hydrogen was injected, and the variation in gas temperature, flow rate and hydrogen concentration were observed at several points in the inner space to analyze the hydrogen elimination effect of the catalysts used.

Specifications of the hydrogen recombination catalysts used are detailed in Table 1-1. Precious metal nanoparticles were sprayed on the wall of a monolithic ceramic substrate having many cells. To optimize the catalyst's shape, several catalysts with different cell densities were prepared. The catalysts were placed in a chimney-shaped tube and installed in the center of the test


**Fig.1-15 Effect of catalyst thickness**

(a) Flow rate was observed for the several catalysts. (b) The flow rate did not decrease even when using the thicker catalyst on a sample with the cell density of 0.047.

equipment. The reaction began after hydrogen injection. Because the reaction between hydrogen and oxygen is exothermic, gas convection proceeds upward through the chimney-shaped tube, reducing the hydrogen concentration in the entire space. The catalytic performance was determined by examining the flow rate, as illustrated in Fig.1-14. As the cell density decreased, the flow rate increased, i.e., the catalytic performance improved as the cell density of the catalysts decreased. Several samples with varying catalyst thickness were prepared (Fig.1-15(a)); their resulting catalytic performance is shown in Fig.1-15(b). The flow rate did not significantly decrease when the catalyst had a cell density of 0.047, even when the catalyst thickness was increased. Because the reaction itself increased as the thickness increased, these results indicate that a catalyst with a cell density of 0.047 can be effective for large amounts of hydrogen.

In collaborations with synchrotron radiation experiments and numerical simulations, studies aimed at developing more effective hydrogen recombination catalysts and at ensuring safety in waste storage have been promoted.

This work was part of the result conducted “R&D on technology for reducing concentration of flammable gases generated in long-term waste storage containers”, and supported by the Ministry of Education, Culture, Sports, Science and Technology (MEXT), Japan.

### Reference

Ono, H., Matsumura, D. et al., Research on Hydrogen Safety Technology Utilizing the Automotive Catalyst, E-Journal of Advanced Maintenance, vol.11, no.1, 2019, p.40-45.

# 1-7 Estimating Radioactive Waste Inventory

## — Sorption Behavior of Actinides on Zeolite —



**Fig.1-16 A test tube used in the sorption experiment of U and Np**

U or Np is added to the experimental solution containing zeolite. The sorption behavior of U and Np is observed by the change of U and Np concentration in solution with time.

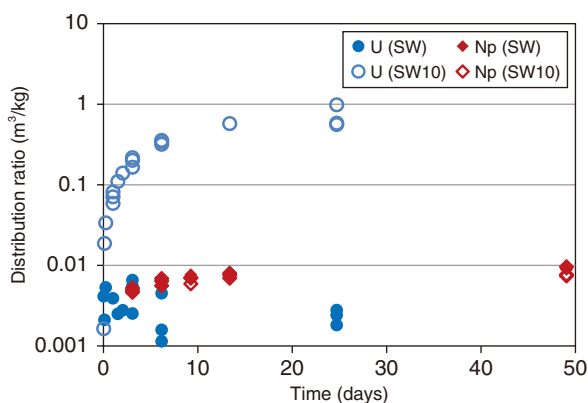


**Fig.1-17 Change in distribution ratio of U and Np with time**

The distribution ratio of U in simulated seawater diluted ten times by deionized water (SW10) was higher than that of Np and U in simulated seawater (SW).

At the TEPCO's Fukushima Daiichi NPS, contaminated water has been processed by water treatment apparatuses to remove radionuclides. Spent zeolite, used as an absorbing material in these apparatuses, is disposed of as radioactive waste. An estimation of the kinds and amount of the radionuclides present in this spent zeolite is necessary for selecting a suitable disposal concept and safety assessment. However, estimation of the inventory via sampling of zeolite from spent zeolite vessels is difficult because of the high dose rate and vessel structure. Therefore, sorption experiments of U and Np on zeolite (IONSIV™ IE-96, UOP), which is used in the water treatment apparatus SARRY, were conducted to develop an inventory estimation method based on the sorption behavior of radionuclides on zeolite (Fig.1-16).

The resulting distribution ratios using simulated seawater (SW) and simulated seawater diluted ten times by deionized water (SW10) are shown in Fig.1-17. Here, the distribution ratio was calculated by dividing the amount of U or Np sorption on zeolite (i.e., solid phase concentration) by the concentration of U or Np in the solution. A high distribution ratio indicates that a large amount of U or Np was sorbed onto the zeolite. The results indicated that a low distribution ratio of U was obtained in SW, whereas the distribution ratio was significantly increased in SW10. Alternatively, the distribution ratio of Np was low and independent of seawater concentration.

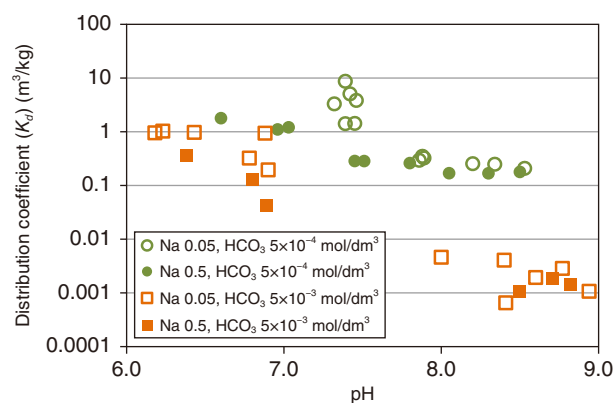


**Fig.1-18 Dependency of uranium distribution coefficient on pH**

The distribution coefficient of U decreased due to the increase in carbonate concentration when the pH was higher than 8. The distribution coefficient was independent of Na<sup>+</sup> concentration.

To clarify the dominant factor causing the variation of the distribution ratio of U between SW and SW10, an experiment was carried out as functions of carbonate and Na<sup>+</sup> concentration in the experimental solution. The resulting distribution coefficient ( $K_d$ ) is shown in Fig.1-18 as a function of the pH, where  $K_d$  is defined as the distribution ratio at sorption equilibrium. In the pH range from 8 to 9, the  $K_d$  of U was low at a higher carbonate concentration, whereas the  $K_d$  was independent of Na<sup>+</sup> concentration. This indicates that the difference in  $K_d$  of U between SW and SW10 is due to the difference of carbonate concentration in the solution. The decreasing  $K_d$  with increasing carbonate concentration may be caused by the increase in the concentration of uranium-carbonate complexes, which have a low sorption ability on zeolite. The  $K_d$  of Np was found to be independent of Na<sup>+</sup> and carbonate concentration. This was consistent with the trend of the distribution ratio of Np observed in the experiment using SW and SW10.

Thus, the carbonate concentration may be a dominant factor in controlling the inventory of radionuclides in spent zeolite.

This work was part of the result conducted “Development of technology for treatment and disposal of accident waste”, and supported by the Agency of Natural Resources and Energy (ANRE), the Ministry of Economy, Trade and Industry (METI), Japan.

### Reference

Ishidera, T. et al., Sorption Behavior of U and Np on Zeolite, Progress in Nuclear Science and Technology, vol.5, 2018, p.221–224.

## 1-8 Towards Routine Analysis of Difficult-to-Measure Radionuclides — Preparation of Analysis Manuals for $^{93}\text{Zr}$ , $^{93}\text{Mo}$ , $^{107}\text{Pd}$ , and $^{126}\text{Sn}$ Waste —

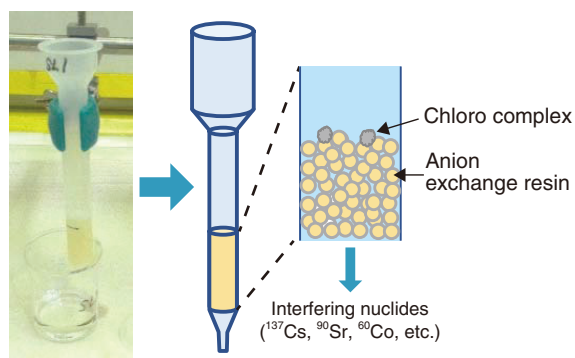


**Fig.1-19 Separation of interfering nuclides using an anion exchange resin**

$^{126}\text{Sn}$  was adsorbed on an anion-exchange resin using hydrochloric acid to separate it from interfering nuclides that do not form complexes with chloride ions.



**Fig.1-20 Planar high purity germanium low-energy photon spectrometer (Ge-LEPS)**

The spectrometer window is made from a thin beryllium film, allowing low-energy photons (e.g.,  $\gamma$ -rays in the case of Sn) to be measured with high efficiency.

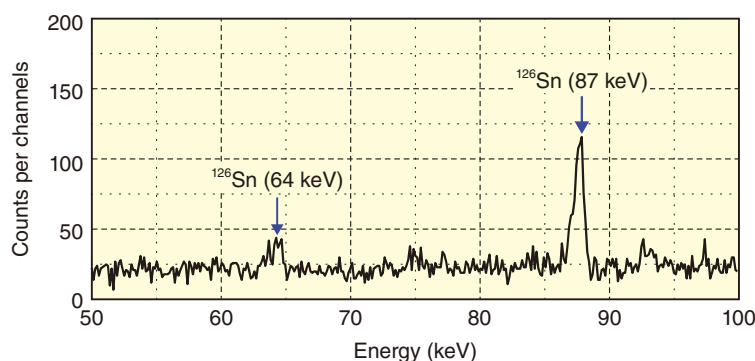


**Fig.1-21  $^{126}\text{Sn}$  measurement spectrum using Ge-LEPS**

Two  $\gamma$ -rays were emitted as a result of  $^{126}\text{Sn}$  decay, shown here as peaks at 64 and 87 keV.

The establishment of waste disposal policies including future waste such as rubble is urgent for proper decommissioning of the TEPCO's Fukushima Daiichi NPS (1F). As such, radioactivity data must be collected, and new analytical methods must be established for nuclides which the analytical methods have not been determined. Analytical methods simple enough to apply during routine analysis for four such nuclides were thus developed: zirconium-93 ( $^{93}\text{Zr}$ ), molybdenum-93 ( $^{93}\text{Mo}$ ), palladium-107 ( $^{107}\text{Pd}$ ), and tin-126 ( $^{126}\text{Sn}$ ).

Among these, the analytical method for  $^{126}\text{Sn}$  is discussed here as an example. A hydrogen peroxide pretreatment was first used to ensure the presence of only tetravalent Sn, as Sn coexists as divalent and tetravalent ions. In a hydrochloric acid solution, Sn forms a chloro complex (i.e., a complex with a chloride ion), becoming an anion that can then be adsorbed on an anion-exchange resin (Fig.1-19) and separated from interfering nuclides that do not become anions, such as cesium-137 ( $^{137}\text{Cs}$ ) and strontium-90 ( $^{90}\text{Sr}$ ), which emit beta rays and raise the background by bremsstrahlung.

The gamma rays were then measured using a planar high-purity germanium low-energy photon spectrometer (Ge-LEPS)

(Figs.1-20 and 1-21).

$^{93}\text{Zr}$  and  $^{93}\text{Mo}$  were adsorbed to a solid-phase extraction agent (TEVA resin) using a weak concentration of hydrofluoric acid, eluted with a high concentration of hydrofluoric acid and hydrochloric acid, and then quantified by mass spectrometry or radiation measurement.  $^{107}\text{Pd}$  was adsorbed to an anion exchange resin using a hydrochloric acid, eluted with ammonia water to efficiently separate from interfering nuclides, and then quantified by mass spectrometry.

The accuracy of the developed analytical method was confirmed using contaminated water collected from 1F. Furthermore, a worker-friendly analysis manual incorporating a check sheet was developed for routine analysis of radionuclides, which is expected to assist the accelerated establishment of disposal policies involving the collecting and accumulating a large amount of radioactivity data when radiochemical analysis is started at the Okuma Analysis and Research Center.

This work was supported by the Subsidy Project of Decommissioning and Contaminated Water Management by the Agency for Natural Resources (ANRE), the Ministry of Economy, Trade and Industry (METI), Japan.

### Reference

Aono, R. et al., Development of  $^{93}\text{Zr}$ ,  $^{93}\text{Mo}$ ,  $^{107}\text{Pd}$  and  $^{126}\text{Sn}$  Analytical Methods for Radioactive Waste from Fukushima Daiichi Nuclear Power Station, JAEA-Technology 2017-025, 2017, 32p. (in Japanese).

# 1-9 Assessing the Safety of Reusing Contaminated Rubble

## — Restricted Reuse in the TEPCO's Fukushima Daiichi NPS Site —

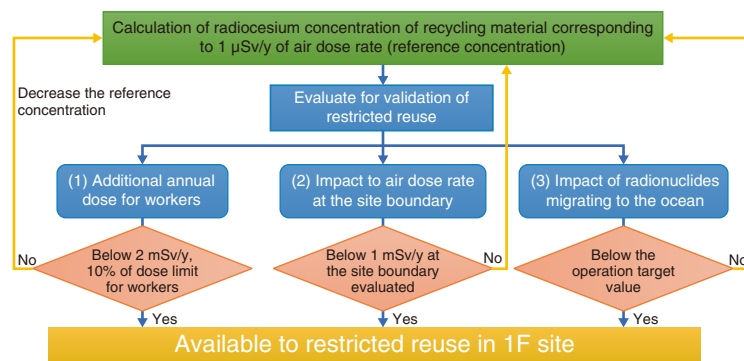


**Fig.1-22 Safety assessment of reuse methodology**

When reusing contaminated rubble, it is important to prevent increasing the dose rate. A validation methodology was constructed considering the current radiation management in 1F site.

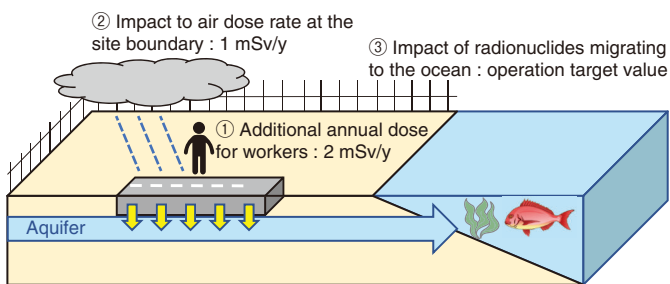


**Fig.1-23 Conceptual diagram for the evaluation of reference radiocesium concentration in restricted reuse as road material**

① The dose to workers should not exceed 10% of the dose limit, ② the increased annual dose by restricted reuse evaluated at the 1F site boundary should not exceed 1 mSv/y, ③ the radionuclide concentration of groundwater migrating from the recycled material should not exceed the operation target value, were confirmed.

A large amount of contaminated rubble from the accident and subsequent activities toward the decommissioning is stored at the TEPCO's Fukushima Daiichi NPS (1F) site. Of the rubble stored outdoors with a surface dosage rate of under 0.1 mSv/h, rubble with a dose rate of less than 5  $\mu$ Sv/h will be recycled and applied in a restricted reuse within the 1F site. Currently, the 1F site is controlled as the existing exposure situation, where had shifted from an emergency exposure situation, and exposure doses of all persons in the 1F site are controlled. There is no precedent for establishing reference values such as dose and/or concentration for reuse of contaminated rubble under the existing exposure situation.

Therefore, a basic approach to estimate the reference radiocesium concentration for a restricted reuse of contaminated rubbles within the 1F site was designed; the used safety assessment of this approach is shown in Fig.1-22. Material was reused when the radiocesium concentration did not significantly increase the air dose rate in the 1F site to reduce any additional exposure dose to workers. The increased dose rate by restricted reuse was capped at 1  $\mu$ Sv/h, which is the minimum dose rate at the 1F site measured by ionization chamber detectors. In addition, in order to validate the reference concentration, we confirm the reuse does not affect the current radiation management in 1F site by three items described below, ① the dose to workers should

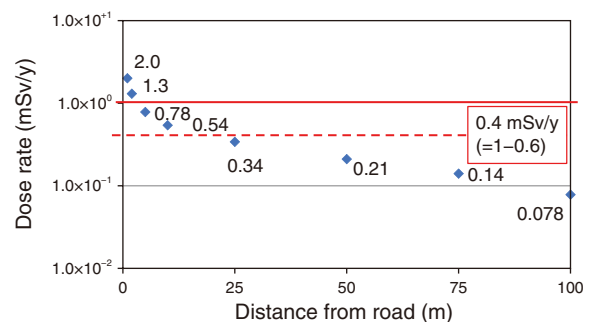


**Fig.1-24 Dose rate corresponding to the distance from the site boundary to the road made of recycled material**  
Considering the margin decided by maximum dose rate (0.6 mSv/y) at the site boundary, the distance necessary for to be under 1 mSv/y on the site boundary was evaluate.

not exceed 10% of the dose limit, ② the increased annual dose by restricted reuse evaluated at the 1F site boundary should not exceed 1 mSv/y, ③ the radionuclide concentration of groundwater migrating from the recycled material should not exceed the operation target value (1 Bq/L for  $^{134}\text{Cs}$  and  $^{137}\text{Cs}$ , 5 Bq/L for all  $\beta$ )(Fig.1-23). When the annual dose at the 1F site boundary and radionuclides concentration in groundwater cannot clear the current radiation management, the distance from the position of reuse to the boundary not to exceed the value of the current radiation management can also be evaluated. Target nuclides in these validations include radiocesium,  $^{90}\text{Sr}$ , which is contained in the rubble with 1% concentration against radiocesium, and  $^{14}\text{C}$ , which was contained above the clearance level.

The reference concentration was thus calculated and verified. Road material and building bases were considered for recyclability in 1F. It is shown that the additional dose for worker not exceed 10% of dose limit by reusing for both purposes with reference concentrations. And, we evaluated the distance from the position of reuse to the boundary not to exceed the value of the current radiation management by reusing. (Fig.1-24).

This study was partly sponsored by the Secretariat of the Nuclear Regulation Authority (NRA), Japan.

### References

- Shimada, T., Miwa, K. et al., Study on Restricted Use of Contaminated Rubble on Fukushima Daiichi NPS Site (1) Estimation of Reference Radiocesium Concentration for Recycling Materials, Progress in Nuclear Science and Technology, vol.6, 2019, p.203–207.
- Miwa, K. et al., Study on Restricted Use of Contaminated Rubble on Fukushima Daiichi NPS Site (2) Validation of Reference Radiocesium Concentration for Recycling Materials, Progress in Nuclear Science and Technology, vol.6, 2019, p.166–170.

# 1-10 Development of Robot Simulator for Decommissioning Task Training — Multi-Copter Simulator and Virtual Operator Proficiency Training System —

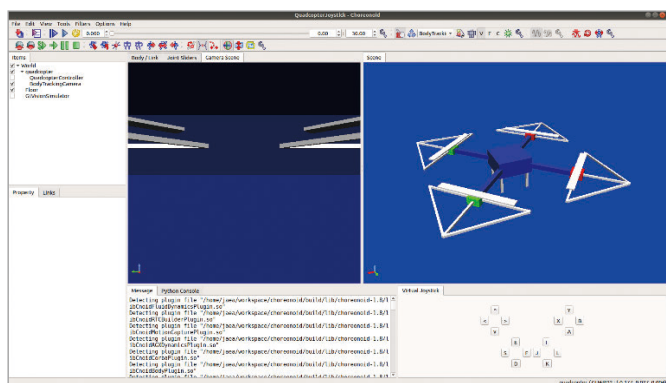


**Fig.1-25 Example screen of a multi-copter simulation**

A mounted camera view and bird's eye view are on the center and right, respectively.

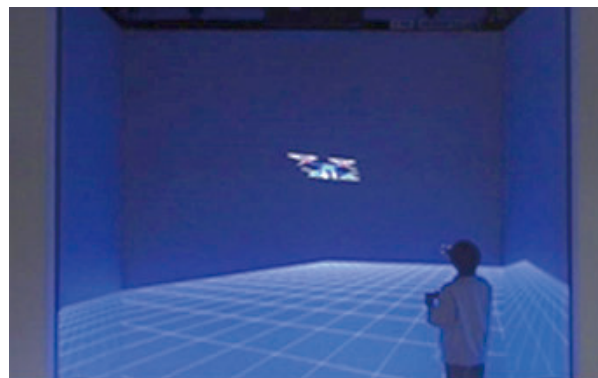


**Fig.1-26 Virtual operator proficiency training**

An example training using a virtual reality system

Due to the high radiation doses present since the accident at the TEPCO's Fukushima Daiichi NPS (1F), radiation and physical survey tasks have been executed with remotely operated robots. However, maneuvering these remotely operated robots and executing the tasks safely are difficult due to unexpected environmental conditions in the reactor building. As such, specialized robots must be developed and operators must be trained. A robot simulator to support the design of remotely operated robots and operator proficiency training is thus under development.

Recently, a multi-copter was used to perform a radiation survey in the reactor building. Maneuvering a multi-copter in this indoor environment is difficult, as its behavior is affected by the local fluid dynamic interactions with nearby structures. An operator proficiency training for maneuvering the multi-copter is also required to cope with such situation. A simulator used to calculate the physical behavior of a multi-copter and a 3D real-size projection system for multi-copter operation training is thus under development.

The simulator determines the behavior of the flying multi-copter by calculating the effect of buoyancy and fluid resistance on the body of the multi-copter, as well as the Coanda and ground effects. The Coanda effect is a phenomenon in which a fluid jet is attracted to the surface of a nearby object such as a wall or ceiling,

whereas the ground effect is a phenomenon in which lift increases near the ground. These effects are important because they make maneuvering the multi-copter difficult. We implemented these effects by introducing a simple calculation model.

A full-scale simulated world projection system in real-time was also designed to provide a realistic training experience to an operator. This system was implemented utilizing the commercial application EasyVR to project the simulated world to a cave-type virtual reality screen and the GL-DLL commercial application Fusion to transfer the simulator's OpenGL (Open Graphics Library) rendering signals to EasyVR. An example view of a multi-copter simulation is shown in Fig.1-25, and an example virtual operator proficiency training is shown in Fig.1-26. Using the simulator and projection system allowed the behavior of a multi-copter in an indoor environment to be calculated in real-time, and projecting the results in 3D allowed for better operator proficiency training.

Future work will focus on extending the operator proficiency training to other required functions in contribution to the decommissioning of 1F.

The presented development is a part of the result of "Development of a Robot Simulator for Mockup Plants", supported by Fukushima Prefecture. This research was commissioned by FSK Co., Ltd. in 2017.

## Reference

Suzuki, K. et al., Development of a Multi-Copter Simulator and a Projection System for Virtual Operation Experience, Proceedings of 2019 IEEE/SICE International Symposium on System Integration (SII 2019), Paris, France, 2019, 6p., in USB Flash Drive.

# 1-11 Observed Decrease of Radiocesium in River Water

## — Result of Three-Year-Long Observation —

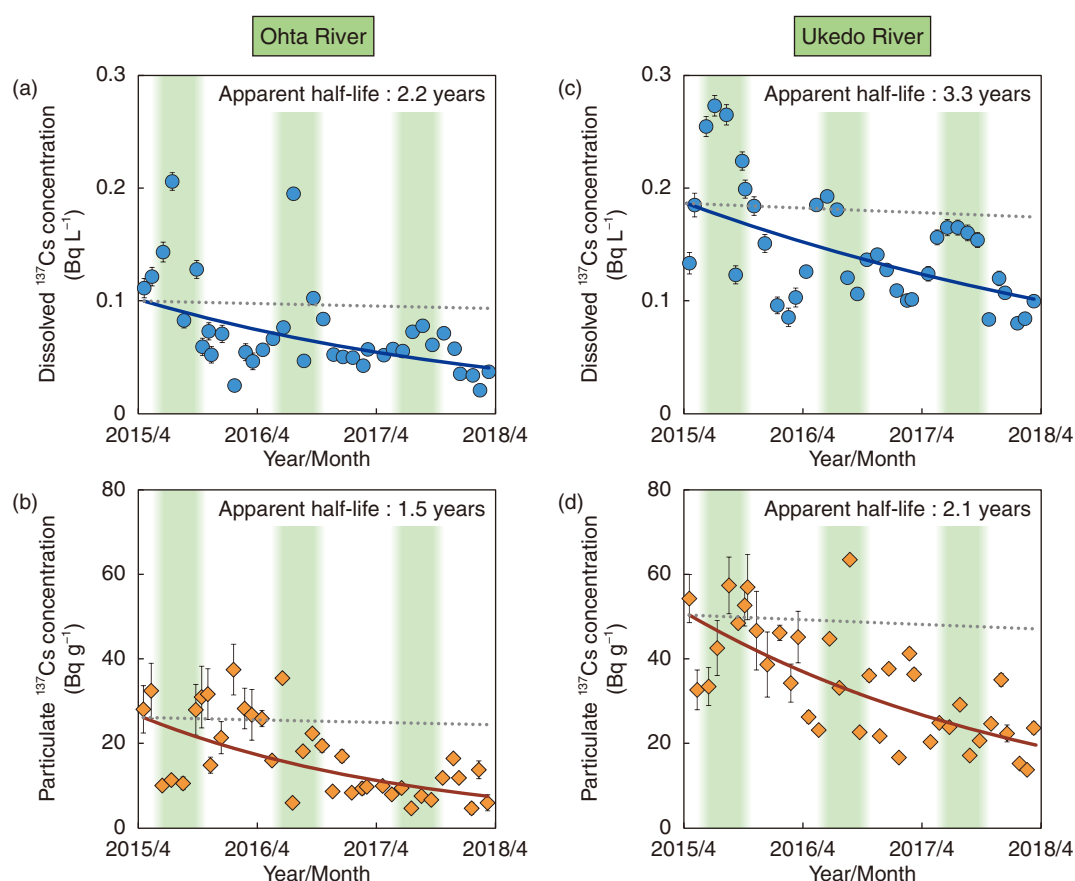


**Fig.1-27 Dissolved and particulate  $^{137}\text{Cs}$  concentrations in river water**

Temporal variations in the concentrations of (a) dissolved  $^{137}\text{Cs}$  and (b) particulate  $^{137}\text{Cs}$  in the Ohta River, and (c) dissolved  $^{137}\text{Cs}$  and (d) particulate  $^{137}\text{Cs}$  in the Ukedo River. The  $^{137}\text{Cs}$  concentrations (solid lines) declined more rapidly than physical decay (dotted lines). Green areas correspond to summertime. The error bars represent the combined uncertainty of measurements.

Radiocesium (RCs) resulting from the accident at the TEPCO's Fukushima Daiichi NPS is transported by river system. A survey of river water by the Ministry of the Environment has suggested that RCs has not been detected (detection limit:  $1 \text{ Bq L}^{-1}$ ). However, the detected RCs concentration in some freshwater fish has been higher than the Japanese limit of  $100 \text{ Bq kg}^{-1}$  for general foodstuffs. To understand the mechanism of RCs uptake by freshwater fish and understand when fishing can be resumed, the RCs concentration and variation in river water must be understood. Therefore, the  $^{137}\text{Cs}$  concentration in river water was observed from four to seven years after the accident, revealing a declining trend.

Water samples from the Ohta and Ukedo rivers in the eastern Fukushima Prefecture were thus collected monthly and filtered through  $0.45\text{-}\mu\text{m}$ -pore size membrane filters from April 2015 to March 2018. The  $^{137}\text{Cs}$  concentrations were determined by  $\gamma$ -spectrometry using Ge-detectors coupled with multi-channel analyzers for particulate fractions on the membrane filters and dissolved fractions that passed through the filters. The dissolved fraction was concentrated to lower the detection limit of  $^{137}\text{Cs}$ .

As a result, the dissolved and particulate  $^{137}\text{Cs}$  concentrations in river water were observed to be in decline (Fig.1-27). The apparent half-lives of dissolved and particulate  $^{137}\text{Cs}$  concentrations estimated by an exponential decay model were 2.2 and 1.5 years, respectively, for the Ohta River (Figs.1-27(a) and (b)) and 3.3 and 2.1 years for the Ukedo River, respectively (Figs.1-27(c) and (d)). These observed decrease rates were 10 times faster than physical decay (half-life: 30.1 years). This suggests that the amount of RCs discharged from the land is decreasing with time.

Furthermore, the dissolved  $^{137}\text{Cs}$  concentration increased in the summer (Figs.1-27(a) and (c)). Because RCs contained in litter and soil organic matter elutes by decomposition, the dissolved  $^{137}\text{Cs}$  concentration might increase in the summer when decomposition is active. However, the increase of  $^{137}\text{Cs}$  concentration in summer has decreased, indicating that the RCs discharged from land is decreasing with time.

The results of this study promote the understanding of the medium- and long-term impacts for RCs concentration in river water and freshwater fish.

### Reference

Nakanishi, T. et al., Trend of  $^{137}\text{Cs}$  Concentration in River Water in the Medium Term and Future Following the Fukushima Nuclear Accident, *Chemosphere*, vol.215, 2019, p.272–279.

# 1-12 Radiocesium Behavior from Forest to Stream Water and River

## — Understanding How Dissolved Radiocesium is Discharged from Upstream —

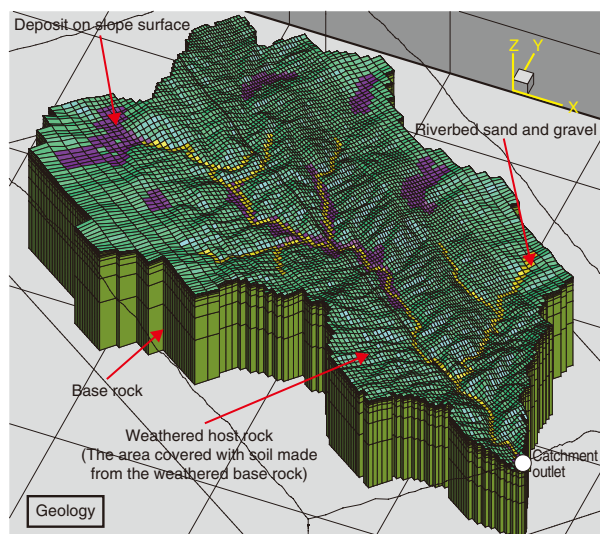


**Fig.1-28 3-D-structure of the studied area**

Watershed hydrological modeling (GETFLOWS) simultaneously simulates the surface and subsurface water using a 3D model based on the hydrogeological data and a 2D model based on digital elevation data. The radiocesium behavior in the environment was predicted by calculating sediment and radiocesium transport based on the obtained water velocity of the studied area.

Approximately 70% of the radiocesium (hereafter  $^{137}\text{Cs}$ ) fallout to terrestrial area from the TEPCO's Fukushima Daiichi NPS accident occurred in forest areas where decontamination work has not yet been done. Studying the behavior of  $^{137}\text{Cs}$  from the forest to stream and river waters is thus required to understand how the  $^{137}\text{Cs}$  concentration in agricultural products and freshwater ecosystems have changed. This includes understanding the discharge of  $^{137}\text{Cs}$  adsorbed by soil particles (i.e., particulate  $^{137}\text{Cs}$ ) but also bio-available  $^{137}\text{Cs}$  in water (i.e., dissolved  $^{137}\text{Cs}$ ). Therefore, water, sediment, and  $^{137}\text{Cs}$  transport were simulated using a watershed model of the 99% forest area (in Minamisoma city and Namie town, Fig.1-28), upstream of the Ohta River catchment, in GETFLOWS. The simulated results were then compared with observed dissolved  $^{137}\text{Cs}$  upstream discharge behavior.

The reproducibility of models related to water and sediment discharge at the discharge point were first confirmed, as shown in Fig.1-28. The partitioning of the  $^{137}\text{Cs}$  inventory between the particulate and aqueous phases occurred instantaneously and was modeled with the distribution coefficients ( $K_d$ ). In the first simulation (case 1), the  $K_d$  was based on the partitioning between the dissolved and particulate  $^{137}\text{Cs}$  measured from river water samples taken at simulation area. In the second simulation (case 2), the  $K_d$  dataset was more realistic in its modeling  $^{137}\text{Cs}$

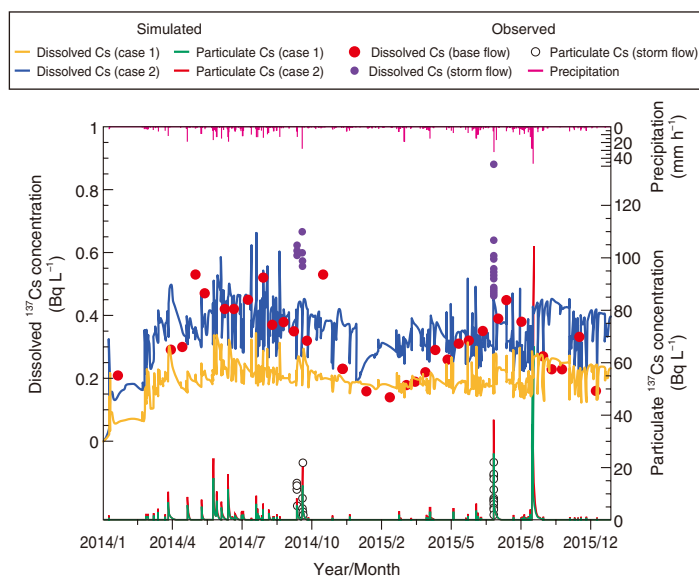


**Fig.1-29 Simulated dissolved and particulate  $^{137}\text{Cs}$  concentration in river water**

Six particle sizes, including clay, silt, fine sand, sand, coarse sand, and gravel, were modeled using GETFLOWS. The distribution coefficients ( $K_d$ ) for the four fine fractions of particle sizes (case 1) were set at 200000 L/kg and, the  $K_d$  value (case 2) were set at 200000 L/kg for clay and silt and 50000 L/kg for fine sand and sand.

absorption to the particulates, as absorption occurs more readily to the finer than coarser grades.

The simulated dissolved and particulate  $^{137}\text{Cs}$  in the river water from January 2014 to December 2015 at the discharge point is shown in Fig.1-29. The case 1 simulation results (—) underestimated the observed dissolved  $^{137}\text{Cs}$  concentration under base flow conditions (0.14–0.53  $\text{Bq L}^{-1}$ , mean: 0.32  $\text{Bq L}^{-1}$ ); however, the case 2 simulation results (—) matched the observations more closely (mean: 0.36  $\text{Bq L}^{-1}$ ). Thus, this model was determined to accurately reproduce the mean dissolved  $^{137}\text{Cs}$  concentration under base flow conditions.

However, neither the seasonal variability in the base flow of the dissolved  $^{137}\text{Cs}$  concentration (●), nor the peaks in concentration that occurred during storms (●), could be reproduced with the simulation parameters used. As well as the results of field monitoring in river, these discrepancies may have been caused an additional input of  $^{137}\text{Cs}$  to rivers by the leaching of organic matter in forest litter, i.e., its process is considered to be other mechanism except for the equilibrium between dissolved and particulate  $^{137}\text{Cs}$ .

Future work will aim to verify and improve this simulation method by further field monitoring and experimental work to reveal the mechanisms of the dissolved  $^{137}\text{Cs}$  leaching process from forest litter to stream and river waters.

### Reference

Sakuma, K. et al., Applicability of  $K_d$  for Modelling Dissolved  $^{137}\text{Cs}$  Concentrations in Fukushima River Water: Case Study of the Upstream Ota River, Journal of Environmental Radioactivity, vols.184–185, 2018, p.53–62.

# 1-13 Clarifying the Distribution of Sediment-Associated Radiocesium at the Bottom of a Pond without Sediment Sampling — Visualizing the Vertical Distribution of Sediment-Associated Radiocesium —

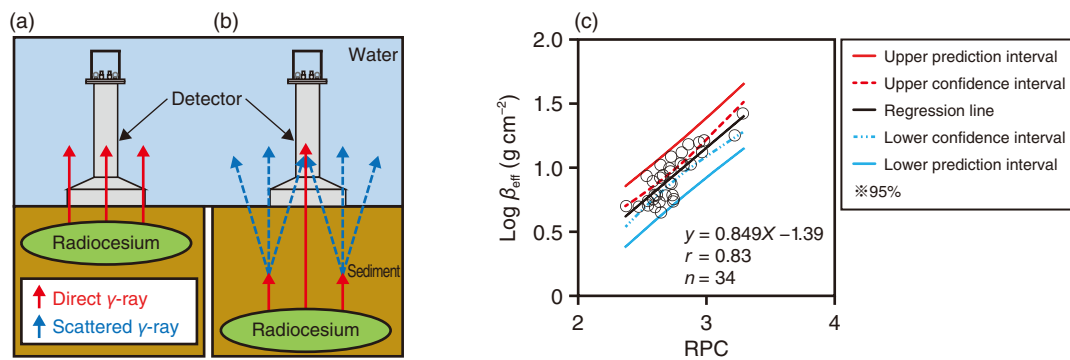


**Fig.1-30 Measuring the gamma-ray spectra of surface sediment**

(a) The contribution ratio of direct gamma rays emitted from radiocesium was high when radiocesium was emitted from the surface-layer sediment. (b) The contribution ratio of scattered gamma rays was high when radiocesium was emitted from deeper-layer sediment because the emitted gamma rays were shielded by soil particles. (c) Relationship between RPC obtained by in-situ measurement and  $\beta_{\text{eff}}$  obtained by sediment sampling.

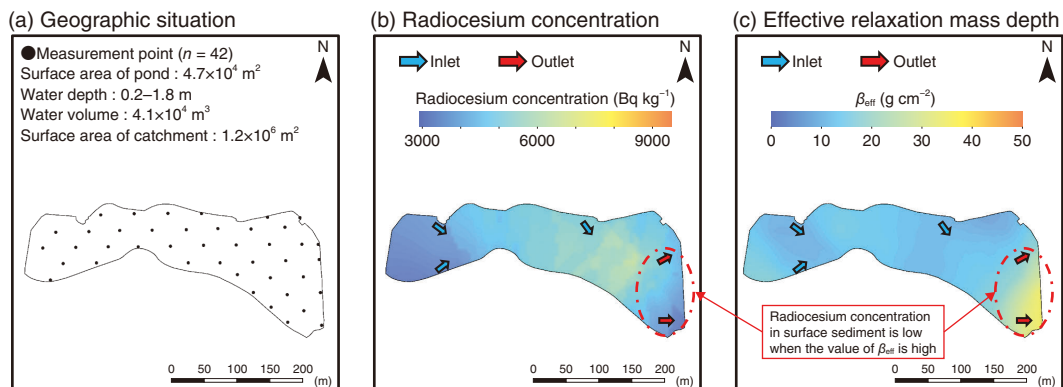


**Fig.1-31 Applying the model to a real pond**

(a) Measured gamma-ray spectra at the pond bottom, used to estimate the (b) radiocesium concentration of the surface sediment and (c) vertical distribution of radiocesium.

Knowing the distribution of sediment-associated radiocesium at the bottom of a pond is necessary for understanding how to decontaminate, dredge, and restart agricultural activities. The vertical distribution of radiocesium must be understood to dredge the sediment effectively. However, obtain these data is difficult and time-consuming. A radiation measurement method using a waterproof detector has thus been developed to investigate the distribution of sediment-associated radiocesium at the bottom of a pond rapidly and easily. However, this method only allows for the measurement of the radiocesium concentration in surface sediment. Therefore, a method to estimate the vertical distribution of sediment-associated radiocesium was developed to focus on the characteristics of the gamma-ray spectrum (scattered and direct) obtained from the surface sediment at a pond bottom (Fig.1-30).

It is estimated that the contribution ratio of direct and scattered gamma-ray is varied with the depth from which radiocesium is emitted. To confirm this, 253 data points regarding the characteristics of the gamma-ray spectrum and vertical distribution of radiocesium in 64 pounds of sediment samples in the Fukushima Prefecture were collected. A waterproof NaI(Tl) scintillation detector (A-Sub: Hitachi, Ltd.) was dropped into the pond and then used to measure the gamma-ray spectrum for

2 min. The sums of counting rate in scattered peak (150–250 keV) and that in photo peak (550–850 keV) based on the obtained gamma-ray spectra were calculated, respectively. The ratio of sum of counting rate in scattered peak to that in photo peak (RPC) was calculated. Core sediment samples (5–40 cm) were also sampled using a sediment sampling tube. The samples were divided into 5 cm intervals. The parameter regarding the vertical distribution of radiocesium (effective relaxation mass depth ( $\beta_{\text{eff}}$  g cm<sup>-2</sup>)) was calculated based on the measuring result of samples using Ge semiconductor detector.

Positive correlations between RPC and  $\beta_{\text{eff}}$  were observed (Fig.1-30(c)), indicating that the vertical distribution of sediment-associated radiocesium can be estimated via this detector by focusing on the characteristics of gamma-ray spectrum. Forty-two gamma-ray spectra were measured to cover the entire pond (Fig.1-31(a)), allowing a map of the radiocesium concentration in the surface sediment (Fig.1-31(b)) and  $\beta_{\text{eff}}$  (Fig.1-31(c)). As a result, the three-dimensional distribution of sediment-associated radiocesium can be more easily determined using this in-situ measurement than conventional methods. These results will further dredging and restarting the agricultural activities of ponds in the evacuation zone.

## Reference

Ochi, K. et al., Development of an Analytical Method for Estimating Three-Dimensional Distribution of Sediment-Associated Radiocesium at a Reservoir Bottom, *Analytical Chemistry*, vol.90, no.18, 2018, p.10795–10802.

# 1-14 Exploring the Migration of Radionuclides to the Deep Ocean

## — Elucidation of Subduction from the Vertical Distribution of Concentration —

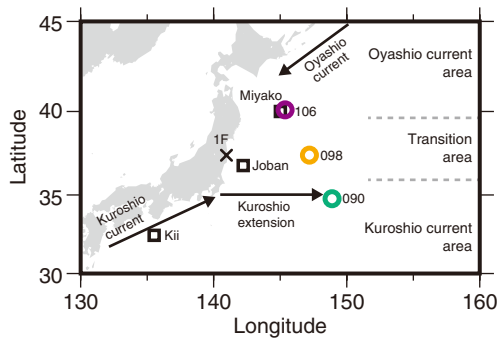


**Fig.1-32 Seawater sampling locations**  
 ○, ●, and □ indicate seawater sampling locations after and before the accident, respectively.

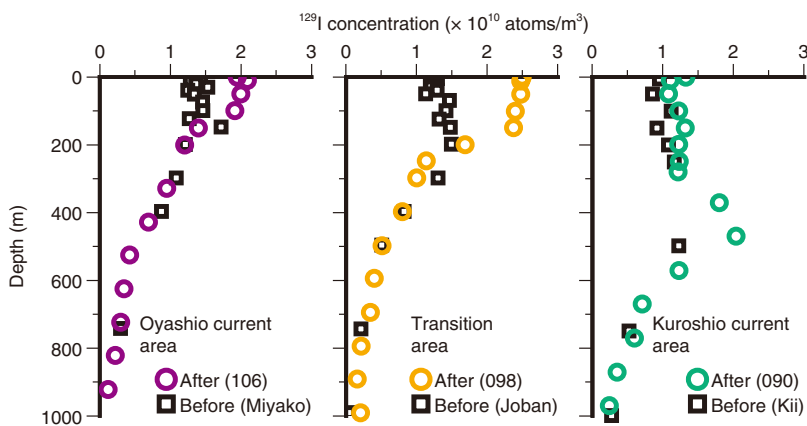


**Fig.1-33 Vertical distribution of  $^{129}\text{I}$  in each oceanic area before and after the accident**

Accident-derived  $^{129}\text{I}$  was present at the surface layer of the Oyashio current and the transition area and was subducted at a depth of around 400 m in the Kuroshio current area.

The accident at the TEPCO's Fukushima Daiichi NPS (1F) released radionuclides into the ocean. Many researches were carried out to understand the migration of radionuclides in the ocean. However, as many of these researchers have focused on the migration of radionuclides within surface layer, this work aimed to study the migration of radionuclides to deep layer.

As many deep-seawater samples were required to do so, a radionuclides detectable from a small sample volume was desired. Therefore, the vertical distribution of iodine-129 ( $^{129}\text{I}$ ) was studied, as  $^{129}\text{I}$  is detectable from 1 L of seawater using accelerator mass spectrometry; radiocesium ( $1 \text{ Bq/m}^3$ ) detection requires 20 L of seawater. In the western North Pacific Ocean, the Oyashio and Kuroshio currents move from north and south, respectively, and provide the transitional seawater between two currents. To clarify the depth profile in the western North Pacific, seawater samples were collected from surface to a depth of 1000 m within the Oyashio current, Kuroshio current and transition areas (Fig.1-32).

The resulting depth profiles of  $^{129}\text{I}$  are shown in Fig.1-33,

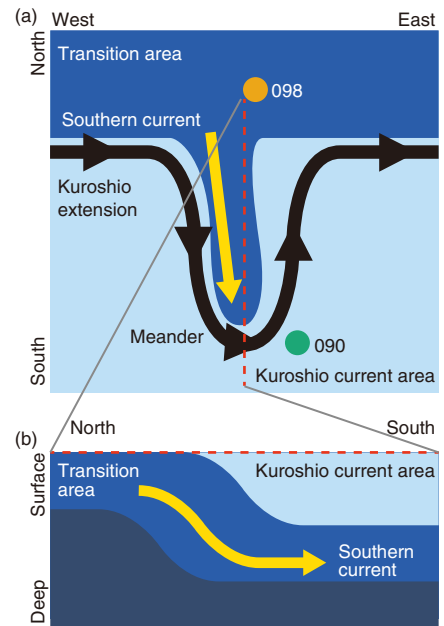


**Fig.1-34 A conceptual diagram of the reproduced seawater current**

(a) Studying the horizontal current showed that seawater in the transition area flowed south (→) induced by the meander of the Kuroshio Extension current (→). (b) Studying the vertical current indicated that the southern current (→) was subducted under the seawater of the Kuroshio current area.

including data regarding the depth profiles of  $^{129}\text{I}$  before the accident. Comparing between the vertical distribution before and after the accident demonstrates a clear increase in concentration caused by the 1F accident occurred from the surface to 150 m and 200 m depth at the Oyashio current and transition areas, respectively, and in the subsurface layer around a depth of 400 m at the Kuroshio current area. To elucidate the subduction to the subsurface layer, the seawater flow was analyzed using a data set that reproduced the flow velocity. As a result, the Kuroshio Extension current which was left from offshore of Chiba was meandering, and a southern current from transition area occurred by the influence of the meander and the southern current was subducted under the seawater of the Kuroshio current area, as the seawater density of the southern current was higher than that of the Kuroshio current area (Fig.1-34).

These results led to the discovery of new oceanographic findings that the radionuclides released by the 1F accident subducted rapidly due to the influence of the meander of the Kuroshio Extension.

### Reference

Suzuki, T. et al., Vertical Distribution of  $^{129}\text{I}$  Released from the Fukushima Daiichi Nuclear Power Plant in the Kuroshio and Oyashio Current Areas, *Marine Chemistry*, vol.204, 2018, p.163–171.

# 1-15 Quickly and Accurately Measuring Environmental Radiation Levels

## — Advanced Conversion Method for Airborne Radiation Monitoring —

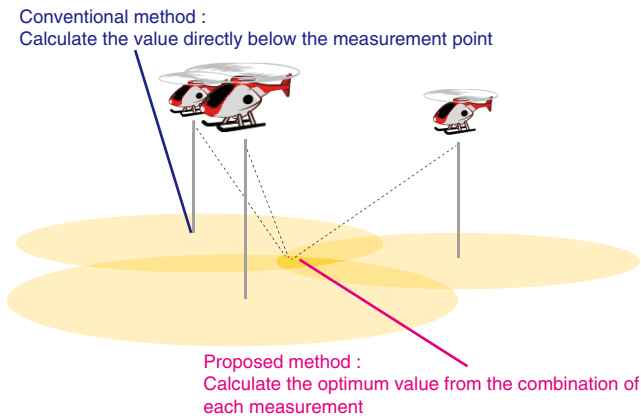


**Fig.1-35 Conventional and proposed radiation measurement method**

The conventional method calculates ground radiation values directly below the measurement point (i.e., point-to-point). The proposed method calculates ground radiation using multiple measured and terrain data (i.e., multi-point-to-point).

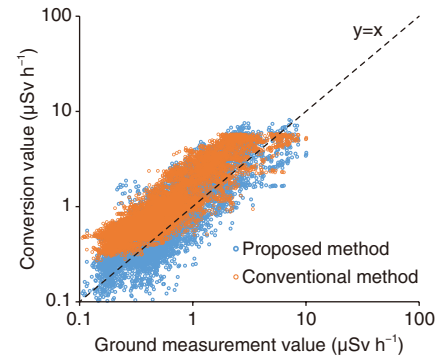


**Fig.1-36 Comparison between conversion value measurement from the sky and ground measurement value**

The actual and calculated dose rate 1 m above the ground using the conventional and proposed methods are shown.

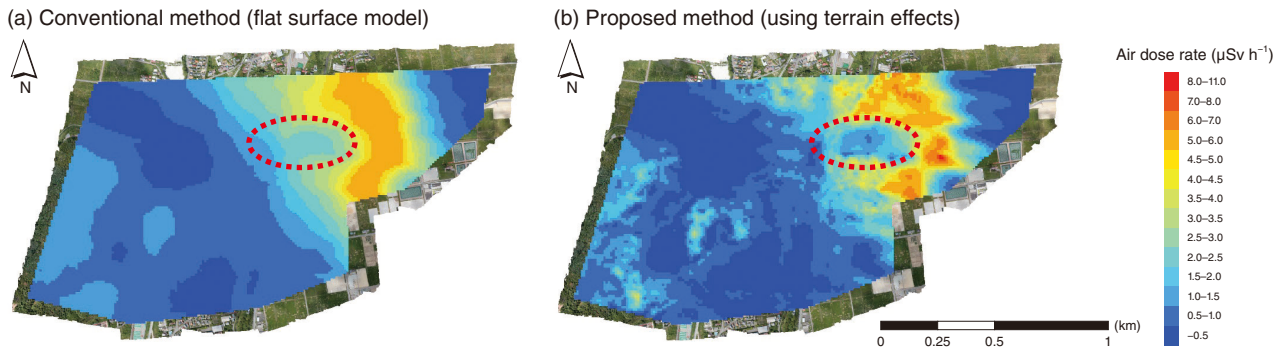


**Fig.1-37 Contour maps of the calculated air dose rate**

Obtained via the (a) conventional and (b) proposed methods. Both convert to 1 m above ground air dose rate.

Since the accident at the TEPCO's Fukushima Daiichi NPS (1F), manned and unmanned helicopters have been used to monitor the radiation levels around the 1F, which are then converted to indicate the dose rate at 1 m above the ground. The conventional conversion method assumes a flat topography and uniform distribution of the radiation, and uses an attenuation factor of radiation by air at the distance between the measurement point and the ground. Therefore, conversion result of actual place, which differs from this assumption, does not match with real ground measurement data. This is especially true in areas of uneven geographical features, shielding by a tree or building, and patchy radiation distribution. An analysis method using the inverse analysis method was thus developed to consider the effects of geographical features and forest shielding in the calculation of dose rate.

The maximum likelihood-expectation maximization (ML-EM) method, used to visualize internal organs in the medical radiation field, was applied. In this method, the optimal distribution of ground values is calculated from many radiation values measured

from the sky (Fig.1-35). An attenuation factor between the radiation source and the detector is calculated by taking into account the thickness of air, trees, and soil based on actual photogrammetry data.

The resulting radiation levels obtained with an unmanned helicopter using the conventional and proposed method are shown in Fig.1-36. Conversion using the proposed inverse analysis method obtained more accurate values than did the conventional method, thus improving the accuracy of conversion from the sky to the ground. Contour maps of the air dose rate obtained by the (a) conventional and (b) inverse analysis method are shown in Fig.1-37, where the red circled area shows a decontaminated area. In the conventional method, the decontaminated area was not clearly visible due to the influence of surrounding radiation, whereas the proposed method more clearly shows the decontamination.

Future work will aim to optimize the parameters of the proposed method and develop an algorithm allowing it to be applied on measurements from both the sky and ground.

### Reference

Sasaki, M. et al., Development of Analysis Method for Airborne Radiation Monitoring Using the Inverse Problem Solutions, Progress in Nuclear Science and Technology, vol.6, 2019, p.63-67.

# 1-16 Evaluating the Effective Dose Based on a Detailed Radiation Map

## — Providing Protection from Radiation in the Specified Reconstruction and Revitalization Base —

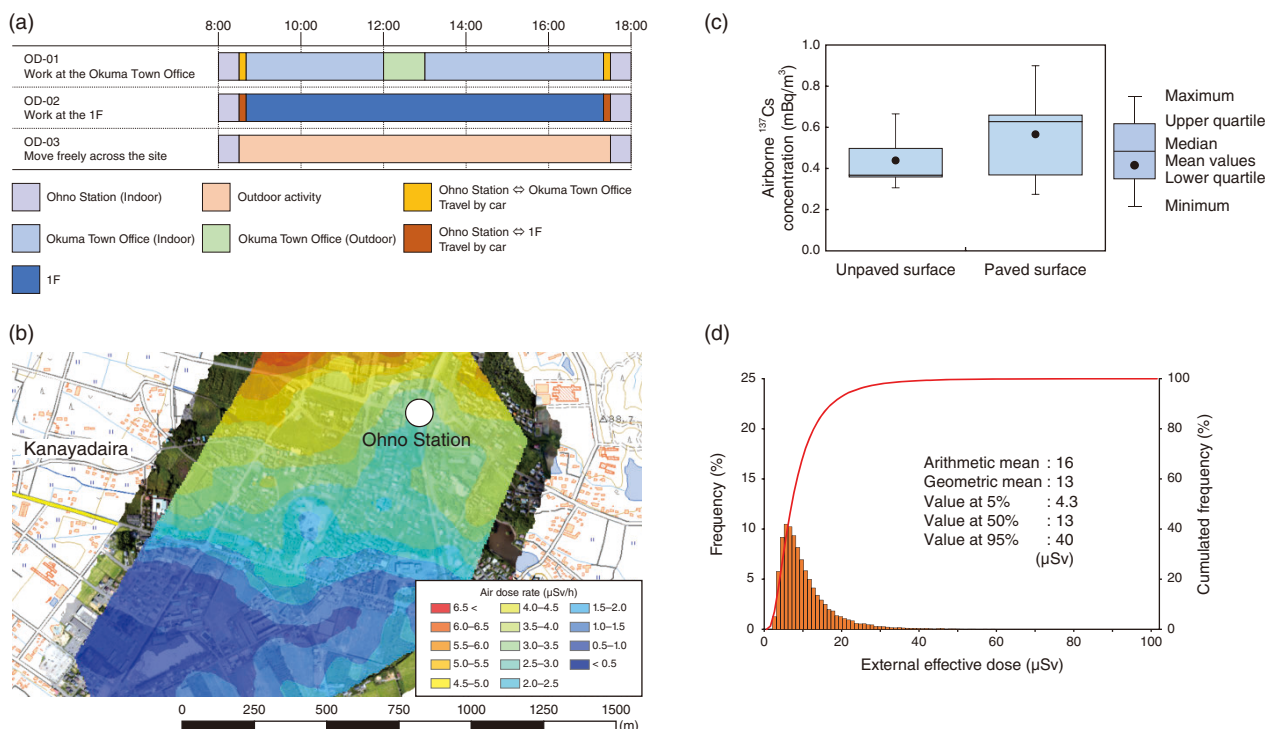


**Fig.1-38 Estimating the effective dose based on detailed radiation monitoring**

- (a) Typical activity patterns assumed in the specified reconstruction and revitalization base in Okuma  
 (b) Distribution map of the air dose rate 1 m above the ground around Ohno Station in Okuma as measured by an autonomous unmanned helicopter  
 (c) Atmospheric concentration of <sup>137</sup>Cs in Okuma collected by dust sampler  
 (d) Estimation of the external effective dose about typical activity pattern at OD-03

The government decided to lift evacuation of part of the high-contamination area affected by the TEPCO's Fukushima Daiichi NPS (1F) accident, where it was anticipated that residents would not be able to return for a long time based on air dose rate. This area, known as the specified reconstruction and revitalization base is located in Okuma, Futaba, and Tomioka around the 1F, where decontamination work and infrastructure improvement have begun and are estimated to be completed in 2023. In these areas: (1) an airborne survey of air dose rate was conducted using an unmanned helicopter, (2) airborne radiocesium was evaluated by collecting air dust and (3) the external/internal effective doses for typical activity patterns were estimated.

First, three types of representative life patterns were developed for each town by interviewing local government officials (Fig.1-38(a)). The exposure dose was estimated following two approaches:

- a deterministic approach, using measuring air dose rate (Fig.1-38(b)) and airborne <sup>137</sup>Cs concentration (Fig.1-38(c)) gained from the specified reconstruction and revitalization base, and

- a probabilistic approach using Monte Carlo calculations considering the distribution of the measured air dose from the base.

The resulting frequency distribution of the number of subjects with evaluated external effective dose ranges about life pattern of OD-03 by Monte Carlo calculations is shown in Fig.1-38(d). The arithmetic mean and value at 95% dose were estimated at approximately 16 and 40 μSv per event (8 h of activity time), respectively. The internal effective dose due to inhalation accounted for less than 1% of the external effective dose.

The exposure dose is expected to be lower in 2023 than determined here by implementing air dose reduction measures such as decontamination work in the specified reconstruction and revitalization base. Future work will aim to continue to optimize the radiation monitoring and exposure assessment, and to conduct realistic evaluations of external/internal dose based on detailed radiation mapping to lift evacuation orders of the specified reconstruction and revitalization base.

### Reference

Funaki, H. et al., Applied Research for the Establishment of Radiation Monitoring and Evaluation of Exposure Dose of Residence at the Zone Designated for Reconstruction and Recovery, JAEA-Research 2018-016, 2019, 48p. (in Japanese).

# 1-17 Modeling the Distribution of Air Dose Rates in Habited Areas of Fukushima Prefecture

## — Developing the 3D Air Dose Rate Evaluation System —

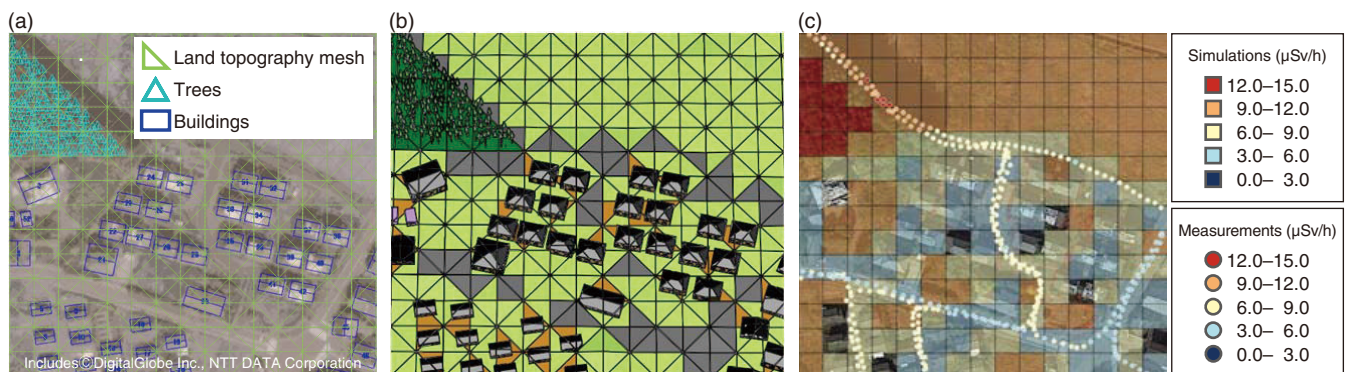


**Fig.1-39 Process of modeling air dose rates with 3D-ADRES**

(a) Selected areas in Fukushima Prefecture are modeled in 3D-ADRES using remote sensing data and satellite imagery. (b) Created models are converted into a format suitable for PHITS. (c) The air dose rate distribution is calculated by simulating the gamma rays emitted by radioactive cesium ( $^{134}\text{Cs}$  and  $^{137}\text{Cs}$ ). The colored squares represent modeled air dose rates, whereas the small colored circles represent air dose rates measured in a person-borne survey. Map imagery © DigiGlobe Inc., NTT Data, Google & Zenrin 2018.

To minimize the external radiation exposure of residents returning to areas where evacuation orders are being lifted after the accident at TEPCO's Fukushima Daiichi NPS (1F) eight years ago, the distribution of air dose rates in inhabited areas must be understood.

Predicting the distribution of air dose rates requires detailed calculations that reflect the differences between the amounts of radioactive cesium ( $^{134}\text{Cs}$  and  $^{137}\text{Cs}$ ) on roads and uncovered surfaces, and the effects of shielding by buildings, trees, and land topography. Previous researchers have made simplifying assumptions, such as assuming completely flat land or ignoring the shielding effect of buildings and trees. To this end, JAEA's Center for Computational Science & e-Systems has worked in collaboration with the Fukushima Environmental Safety Center to develop the 3D-ADRES (3D Air Dose Rate Evaluation System) calculation system. This system was designed to create detailed 3D models of residential areas in Fukushima Prefecture to improve the precision of calculations of air dose rate distributions.

In 3D-ADRES, models are created for a target area by first displaying a satellite image or aerial photograph of the location (Fig.1-39(a)). Digital Elevation Model (DEM) geospatial data are used to create a 3D model of the land surface topography by using a triangular mesh (Fig.1-39(a)). Buildings and trees are added on top of the land topography model with heights determined by the Digital Surface Model (DSM) data, thus creating a realistic model of the target area (Fig.1-39(b)). The model is then converted into a format suitable for the PHITS

code developed by JAEA (Fig.1-39(b)). PHITS uses the Monte Carlo method to simulate the paths taken by gamma rays emitted by radioactive cesium. It models the scattering and changes of direction of gamma rays due to interactions in air, as well as absorption by buildings and trees. In this way, it becomes possible to reproduce the complicated air dose rate distribution around buildings and houses (Fig.1-39(c)). Undertaking radiation transport simulations with PHITS allows for air dose rate distributions for the past, present, and future to be calculated.

3D-ADRES and PHITS were used to calculate the air dose rate distribution in an area near the 1F and to examine the effects of buildings, trees, and asphalt on this distribution. The results indicated that wind and rain easily washes radioactive cesium off of buildings and asphalt roads, thus causing air dose rates approximately 60% lower than expected. This effect was greater than the dose rate reduction that occurs due to the shielding of gamma rays by buildings and trees.

Future work will involve using 3D-ADRES and PHITS to evaluate air dose rates inside rooms in houses and buildings where residents tend to spend long periods of time. The developed model will contribute to minimizing residents' external radiation exposures and predicting the reduction in air dose rates in residential areas over time. Furthermore, modern technologies such as 3D laser scanners and GPS-equipped cameras will be implemented to improve the detail of the models whilst developing automation techniques to streamline model creation.

### Reference

Kim, M., Malins, A. et al., Simulation Study of the Effects of Buildings, Trees and Paved Surfaces on Ambient Dose Equivalent Rates Outdoors at Three Suburban Sites near Fukushima Dai-ichi, *Journal of Environmental Radioactivity*, vol.210, 2019, p.105803-1–105803-10.